OCTOBER 31 2025

Motorboat sound in shallow waters and implications for mitigation $\ensuremath{ igorline{\mathcal{O}} }$

Lucille Chapuis ⁽ⁱ⁾; Michael A. Ainslie ⁽ⁱ⁾; Harry R. Harding; James Campbell; Andrew N. Radford; Stephen D. Simpson; Sophie L. Nedelec



J. Acoust. Soc. Am. 158, 3605–3618 (2025) https://doi.org/10.1121/10.0039578





Articles You May Be Interested In

The effect of boat noise on calling activity in the Lusitanian Toadfish

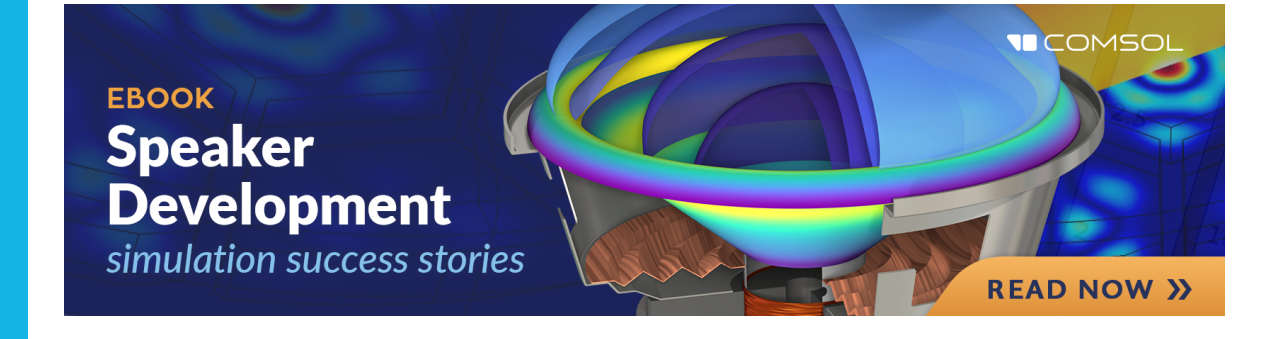
Proc. Mtgs. Acoust. (March 2020)

Underwater single-channel acoustic signal multitarget recognition using convolutional neural networks

J. Acoust. Soc. Am. (March 2022)

Speed dependence, sources, and directivity of small vessel underwater noise

J. Acoust. Soc. Am. (October 2024)









Motorboat sound in shallow waters and implications for mitigation

Lucille Chapuis, ^{1,2,a)} D Michael A. Ainslie, D Harry R. Harding, James Campbell, Andrew N. Radford, Stephen D. Simpson, and Sophie L. Nedelec

ABSTRACT:

Small motorboats are a pervasive source of underwater noise pollution in many coastal regions of the world. The environmental impacts of motorboat noise include marine life disturbances and ecosystem disruptions. Mitigation strategies may involve speed restrictions in certain areas, on the assumption that slower speeds correspond to lower acoustic energy. We investigate the acoustic footprint of small motorboats navigating at different speeds in shallow water. Sound pressure and particle motion are characterized and the source levels estimated. We find that the acoustic energy (source level) associated with small motorboat noise may be higher at low speed than high speed. Our study therefore suggests that the vessel's optimal cruising speed should be considered while implementing speed limitation as a mitigation strategy. © 2025 Acoustical Society of America. https://doi.org/10.1121/10.0039578

(Received 19 March 2025; revised 29 September 2025; accepted 30 September 2025; published online 31 October 2025)

[Editor: James F. Lynch] Pages: 3605–3618

I. INTRODUCTION

Anthropogenic noise affects aquatic fauna in diverse ways (Duarte et al., 2021; Slabbekoorn et al., 2010; Southall et al., 2021) and is defined as a pervasive pollutant in the European Commission, Marine Strategy Framework Directive (2008). Marine traffic is one of the main sources of noise in the ocean (McWhinnie et al., 2017) and has been shown to disrupt the physiology and behavior of marine mammals (Erbe et al., 2019), fishes (Whitfield and Becker, 2014), and invertebrates (Solé et al., 2023). Traffic noise can induce stress, leading to physiological changes, such as hormonal disruptions and metabolic changes in fishes (Graham and Cooke, 2008; Mills et al., 2020; Wysocki et al., 2006) and marine mammals (Holt et al., 2016; Lemos et al., 2022; Rolland et al., 2012). Behaviorally, boat noise can alter conspecific social interactions and communication (Dunlop et al., 2020; Putland et al., 2018; Stanley et al., 2017), elicit avoidance responses (Dyndo et al., 2015; Ivanova et al., 2020; Vabø et al., 2002), and disrupt foraging (Blair et al., 2016; Wisniewska et al., 2018), resting (Mikkelsen et al., 2019), predator responses (Simpson et al., 2016; Wale et al., 2013), and interspecific interactions (Nedelec et al., 2017a). Abatement of anthropogenic noise pollution and mitigation of its effects are vital goals for the protection of sensitive marine habitats; however, studies that

Most studies aiming to characterize vessel sound have focused on large ships and bulk carriers, as they are responsible for most of the traffic noise in the open ocean (Ainslie et al., 2021; Hildebrand, 2009; Wenz, 1962). However, with the development of commercial and recreational activities, smaller motorboats navigating in shallower, coastal waters are increasing in number (Shipton et al., 2025). In addition, shallow coastal zones are home to many of the most biodiverse habitats in the marine environment, including tropical coral reefs, mangroves, kelp, and seagrass zones. Most of the freshwater environment is also shallow. While small motorboats do not produce the intense sounds of large ships, their noise has been shown to disrupt many taxa in these shallow water habitats (Fakan and McCormick, 2019; Ferrari et al., 2018; Harding et al., 2018; Jain-Schlaepfer et al., 2018; Lecchini et al., 2018; McCloskey et al., 2020; Nedelec et al., 2017b). Small boats usually produce sounds in the range 100-800 Hz, a frequency band used by many species for communication, orientation, and predator avoidance (Wilson et al., 2022).

Reducing speed has been described as an effective method for reducing underwater radiated noise from commercial vessels in most cases (MacGillivray *et al.*, 2019). The International Maritime Organization (2014) has recognized that reducing ship speed results in noise reduction (and ship speed reductions have been recommended in some areas) (Chou *et al.*, 2021; Findlay *et al.*, 2023;

¹School of Agriculture, Biomedicine and Environment, La Trobe University, Melbourne 3086, Victoria, Australia

²School of Biological Sciences, University of Bristol, Bristol BS8 1TQ, United Kingdom

³JASCO Applied Sciences (Europe) GmbH, 24223 Schwentinental, Germany

⁴Leibniz-Institute of Freshwater Ecology and Inland Fisheries, Müggelseedamm 310, 12587 Berlin, Germany

⁵Biosciences, University of Exeter, Exeter, Devon EX4 4PS, United Kingdom

fully characterize the noise emitted from vessels, in contexts that are relevant for species that need protection, are scarce.

a)Email: 1.chapuis@latrobe.edu.au

JASA

Putland et al., 2018). For example, slowdowns were used as a trial to reduce the effects of noise on local killer whales (Orcinus orca) in the Salish Sea: the sound reduction was highest in the 10–100 Hz range and achieved a 22% reduction in potential lost foraging time for the whales (Joy et al., 2019). Recently, a decrease in ocean noise levels (a 4dB reduction) was observed likely due to slower commercial ship speeds and fewer ships during the COVID-19 pandemic in the Bahamas (Dunn et al., 2021), a significant reduction also observed almost globally in the deep-ocean during the pandemic in 2020 (Robinson et al., 2023). However, the effect of speed reduction has mainly been observed for large ships in deep waters, and the relation to sound created by small motorboats in shallow waters and their speed is still poorly established.

A few studies have assessed the acoustic pressure signatures of small vessels (<25 m length) in shallow water (<150 m depth) (e.g., Smith et al., 2024; Lagrois et al., 2023; Parsons and Meekan, 2020; Picciulin et al., 2022, Yubero et al., 2025). While vessel speed is widely acknowledged as a key driver of underwater noise levels, the relationship between speed and radiated noise for small boats is not always straightforward. Recent studies have revealed that this relationship can be non-linear due to factors, such as propeller cavitation dynamics, vessel design, and engine performance. For example, Svedendahl et al. (2021) reported that a small boat generated higher noise levels at lower speeds, attributed to increased cavitation when operating outside of its optimal speed range. Similarly, Smith et al. (2024, 2025) observed non-monotonic changes in source levels as speed increased, and linked these patterns to changes in cavitation behavior, particularly in vessels with damaged or fouled propellers. Picciulin et al. (2022) also found that a 10-knot increase in speed for rigid inflatable boats resulted in a ~2-dB rise in broadband source level, suggesting that some vessels may reach a plateau in noise emission beyond certain speeds. These findings highlight the need to consider a range of interacting physical and mechanical variables when assessing small vessel noise, particularly in shallow coastal environments where vessel traffic is intense and diverse.

Aquatic invertebrates and fishes are sensitive to acoustic particle motion, which is difficult to predict from pressure measurements in shallow waters (Nedelec et al., 2016; Popper and Hawkins, 2018). To describe satisfactorily the sound emitted by a motorboat in the context of anthropogenic noise mitigation, it is critical to measure the particle motion in situ, especially in shallow waters where there is not an acoustic free field and the relationship between acoustic pressure and particle motion is complex (Popper et al., 2020). Particle motion magnitude can be calculated from sound pressure when the assumptions of a plane wave or spherical spreading from a monopole source are met. However, in the hydrodynamic near field, or below a duct cut-off frequency, particle motion should be measured or modeled (Nedelec et al., 2021). The cut-off frequency, below which sounds will not propagate as a plane wave and particle motion cannot be calculated from pressure, is related to the water depth, sound speed profile, and sediment composition (Jensen *et al.*, 2011). As a rule of thumb, the need for particle motion *in situ* measurements should be considered at depths of less than 100 m and frequencies lower than 1 kHz (Nedelec *et al.*, 2016, appendix S1).

The aim of this study was to describe the acoustic footprint of a hull and engine type typically used in small motorboats, navigating at different speeds in shallow waters, by using empirical data to characterize the acoustic pressure and particle motion at a fixed receiver. We used measurements of the sound of five approaching 5-m motorboats with 30 hp (~22.4 kW) outboard motors at five different speeds. We investigated the relationship between exposure levels and duration of boat passes, and their relationships with motorboat speed, using the sound pressure exposure levels and particle acceleration exposure levels. The source levels and their power spectral densities were calculated. Finally, we interpreted the results in terms of anthropogenic impacts and boat noise mitigation strategies.

II. METHODS

The international standard for measuring underwater radiated noise in shallow water is ISO 17208-3:2023 (2025). As our measurements and associated processing were carried out during the period 2019–2024, before the publication date of ISO 17208-3:2023 (2025), we developed our own experimental design, with processing based on MacGillivray (2023). The ISO 18405:2017 (2017) terminology for underwater acoustics is followed.

A. Measurement location

This study was conducted from November 19–28, 2019 at Lizard Island Research Station (14° 40' S, 145° 28' E), Great Barrier Reef, Australia, with permission and ethical approvals from Lizard Island Research Station, Great Barrier Reef Marine Park Authority (G39752.1), James Cook University (A2641) and the University of Exeter (eCLESBio000270).

All recordings were made in the bay in front of Lizard Island Research Station, in a sandy-bottom location, from 07:00 to 16:30 local time and only at calm sea state times (Beaufort force 0–2) and without rain. Water temperature ranged from 25.5 °C to 28.2 °C. Tides changed the water levels up to 0.3 m during the experimental procedure.

B. Vessel characteristics and testing scenario

Research station boats were used, each with a $5 \,\mathrm{m}$ length, $2.1 \,\mathrm{m}$ beam aluminum hull for a total mass of $360 \,\mathrm{kg}$ and a $30 \,\mathrm{hp}$ Suzuki outboard 4-stroke engine. The vessels were driven following a straight 200-m line delimited by two buoys (one at the start and one at the end), through a channel formed by the reefs [maximum depth $2.5 \,\mathrm{m}$ (H)], and always by the same driver (H. H.). The recording station was located at the end of the 200-m line, $20 \,\mathrm{m}$ away perpendicularly towards the shore (r) at $1.7-2 \,\mathrm{m}$ depth (h)

depending on the tide (Fig. 1). The driver started the boat pass at the departure buoy and steadily accelerated at full throttle until the target speed was reached (see below), and then maintained this speed until the end buoy was passed. The boat's closest point of approach (CPA) was therefore determined when the boat passed the end buoy, and represented the last sample of the recording. The departure from the end buoy was not recorded, and the following analyses focus on the approach of the boat only. Therefore, only the approach phase of each boat pass (port side) was recorded and analyzed. These acoustic recordings were collected as part of a separate experiment investigating behavioral responses of fish to motorboat noise, where consistent capture of the approach phase was prioritized and the departure was not recorded. The driver used a speedometer application on their mobile phone (Smart GPS Speedometer, AppAspect Technologies Ltd., Bellevue, WA) to monitor the duration and speed of the pass. Boats were driven at five different target speed regimes, initially set in km/h: 6, 12, 18, 24, and 30 km/h. These different target speeds are herein presented in both m/s (respectively corresponding to 1.67, 3.33, 5.00, 6.67, and 8.33 m/s) and knots (respectively: 3.2, 6.5, 9.7, 13.0 and 16.2 knots) and referred to as boat speed "regimes." Each speed plus two control recordings of background ambient noise (hereafter referred to as "ambient noise") were randomly selected inside blocks of seven regimes, so that each speed regime was conducted once before moving to the next replicate to avoid bias according to environmental fluctuations over time (e.g., temperature, sea state, tides).

To measure the depth of the source (d), the center of the propeller hub was used as a reference and its depth measured at each speed by means of a marked reference line. This depth was measured once for each boat regime.

C. Measurement system

Sound pressure was recorded using an omnidirectional hydrophone with inbuilt digital recorder (SoundTrap 300

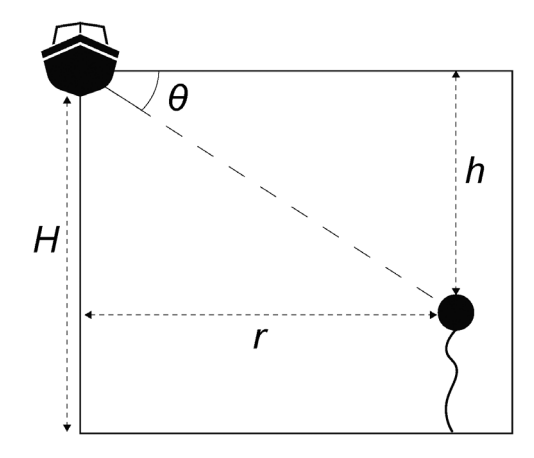


FIG. 1. Measurement geometry for the recordings at Lizard Island, Australia. Solid circle represents recording station (hydrophone and particle motion sensor). H = 2.5 ± 0.2 m (site depth), h = 1.8 ± 0.2 m (sensor depth), r = 20.0 m (horizontal range, i.e., CPA distance), $\theta = \text{grazing angle}$.

STD; response of $\pm 3\,\mathrm{dB}$ over the 20 Hz to 60 kHz; calibrated by manufacturers; Ocean Instruments NZ, Auckland, New Zealand). Five different boats were driven (Ellie, Lili, Marie-Elisabeth, Sarah, and Mary-Ida) in turn. In total, each boat regime was repeated 25 times. Two durations of ambient noise (short and long, see above) were recorded regularly in between boat passes. Trials were stopped and repeated if disrupted by other boats passing less than 500 m away. In total, this resulted in 175 sound pressure recordings (50 ambient and 125 boat recordings).

Sound particle acceleration recordings were made using a triaxial accelerometer (M20-040; measuring range 10-5 kHz; calibrated by the manufacturers; Geospectrum Technologies, Dartmouth, Canada) and a digital 8-track recorder (H6 field recorder; 48 kHz sampling rate, Zoom Corp., Tokyo, Japan). Recording levels from the acquisition system were calibrated using pure sine wave signals from a function generator with a measured voltage recorded in line on an oscilloscope. For particle acceleration recordings, only three of the five different boats (Ellie, Lili, Marie-Elisabeth) were driven in turns with at least two passes for each boat regime, resulting in 30 recordings. Recordings of ambient noise (with no boat pass) were made four times during a 0.6 s ("short") time duration (temporal observation window) and four times during a 3 s ("long") time duration. In total, this resulted in 38 particle acceleration recordings. Sound pressure was recorded simultaneously to all the particle acceleration recordings with the SoundTrap.

D. Data processing

1. Data quality verification

We performed some of the checks required by the standards to ensure the best data quality was used to get our results. We confirmed the proper functioning of the hydrophone and the vector sensor before the deployment and after recovery, thanks to the calibration tones produced by the SoundTrap 300 STD; i.e., the levels recorded were within $\pm 1\,\mathrm{dB}$ from the expected value. Additional verifications were also performed in between recordings to check the vessel speed for each speed regime, the depth of the measurement systems, distance of the CPA, and testing conditions (sea state, tides, rain etc.).

2. Post-processing

All analyses were conducted using paPAM version 2.0.11 (Nedelec *et al.*, 2016), custom-made scripts in MATLAB R2020b and R (R Core Team, 2019).

The recordings were first cropped from the recorded start and end of the boat approaches. The start was identified thanks to a sound stimulus (i.e., knock) created by an observer in the water when the boat started the boat pass at the starting buoy. The end point was clearly identified by a sharp drop in energy visible in both the waveform and spectrogram, which corresponded to the moment the boat crossed the final buoy and the engine was abruptly cut. This transition consistently produced a marked decrease in

JASA

broadband energy across all recordings. Approaches were of different duration depending on the boat speed. Example spectrograms were created with 2048 Hann windows (window duration 42.67 ms) and 50% overlap, representing each of the boat regimes and an ambient recording, both in particle acceleration (magnitude; 10–5000 Hz) and sound pressure (20–24 000 Hz).

For the rest of the analyses, the last 5 m of each boat approach was selected as a data window length (3 s for 3.2 knots, 1.5 s for 6.5 knots, 1 s for 9.7 knots, 0.75 s for 13.0 knots, and 0.6 s for 16.2 knots), as well as samples of 0.6 and 3 s of ambient noise. For sound pressure recordings, the data were first bandpass filtered three times: (1) with third-order Butterworth filter from 10 to 5000 Hz (to allow for comparison with particle motion measurements, limited by hardware frequency sensitivity); (2) from 8.91 to 8910 Hz (corresponding to the ADEON three-decade band BD (Ainslie et al., 2018; ISO 7605:2025, 2025); and (3) from 8910 to 22400 Hz (corresponding to the rest of the frequencies rounded to the nearest decidecade band edge frequency). Mean-square sound pressure level $(L_{n,rms})$, zeroto-peak sound pressure level $(L_{p,pk})$, and sound exposure level (L_E) were computed for each sound pressure recording, and then averaged for each boat regime. Similarly, particle acceleration level ($L_{a,rms}$), and acceleration exposure level $(L_{E,a})$ were calculated from the particle acceleration recordings filtered with third-order Butterworth filter from 10 to 5000 Hz, integrated over the time of each cropped sound (corresponding to the last 5 m to CPA, e.g., 3 s for 3.2 knots) and averaged for each boat regime. All averaging of acoustic metrics (e.g., $L_{p,rms}$, $L_{a,rms}$, L_{E} , $L_{E,a}$) was performed in the linear domain prior to transformation into decibels (dB).

In addition to energy-based metrics, we also calculated kurtosis of the time-domain waveform for sound pressure. This was done using the definition of sound pressure kurtosis provided in ISO 18405:2017 (2017), which describes it as a dimensionless measure of the impulsiveness of a signal. We followed the analytical approach outlined in Müller *et al.* (2020), where kurtosis is used to assess the prominence of transient events in underwater sound. High kurtosis values indicate that the signal contains bursts or spikes, which may be more ecologically disruptive than steady-state signals of similar average energy.

We investigated the relationships between sound pressure level (L_p) and particle acceleration level (L_a) with boat speed regime by fitting a locally estimated scatterplot smoothing model using the "geom_smooth": function in the ggplot2 (Wickham, 2016) package in R. This approach enabled us to visualize nonlinear trends in acoustic energy as a function of speed, with confidence intervals derived from model variance.

We calculated power spectral density (PSD) with a Hann window length of 24 000 samples (2 Hz resolution, i.e., window duration 0.5 s) with a 50% overlap. We calculated the signal-plus-noise-to-noise level difference of each boat regime in order to compare the measured level of the vessels under test to the background noise (i.e., ambient

sound) at the approximate time of the test. As the signal-plus-noise-to-noise ratio was greater than 3 dB and the background noise stable over the recordings (i.e., no changes in environmental conditions, sea state, vessel traffic at the site), following ISO 17208-1 (2016), we adjusted the measurements by removing the background noise power from the initial recorded signal power.

Several analytical approaches exist for calculating propagation loss in shallow-water vessel-noise measurements. For example, Yubero *et al.* (2025) recently proposed the smoothed semi-coherent image method, which improves upon the seabed critical angle method recommended in the draft ISO 17208-3:2023 (2025) standard by reducing bias at mid to high frequencies (\gtrsim 500 Hz) while maintaining robustness at low frequencies. We adopted the propagation loss and source-level estimation procedures from the seabed critical angle method as described in MacGillivray *et al.* (2023), and the propagation loss ($N_{\rm PL}$) was estimated for cylindrical spreading (assuming $H \ll \psi r$) as follows:

$$N_{\rm PL}(r,f) = 10\log_{10} \frac{Hr/(2\psi)}{r_0^2} dB + 10\log_{10} \left(1 + \frac{3c^2}{8\pi^2 f^2 d^2 \sin^2 \psi}\right) dB, \qquad (1)$$

with r as horizontal range (20.0 m), r_0 as the reference distance (1 m) (ISO 1683:2015, 2015), H as water depth $(2.5 \,\mathrm{m}), \, \psi$ as the critical angle for sand $(0.5), \, d$ as the source depth (i.e., propellor depth), f as the acoustic frequency, and c as the speed of sound in water (1480 m/s). We considered this the most appropriate formula available at the time of our processing. Equation (1) has the same high-frequency limit at the smoothed semi-coherent image method, and departs at low frequency from smoothed semi-coherent image by a factor $\sin \psi / (1.0178 \, \psi) \approx 0.942$, corresponding to a difference of 0.3 dB. The largest difference, about 1.6 dB, occurs between 800 and 900 Hz, depending on the precise source depth. Our source level measurements are likely to overestimate the true values in the frequency range 150 to 3000 Hz by up to 1.6 dB. Outside this frequency range, the discrepancy is less than 0.4 dB.

 $N_{\rm PL}$ was thus calculated for each 2 Hz frequency band and the source level (L_s) at each frequency band then calculated via the following:

$$L_{\rm S} = L_p(f) + N_{\rm PL}(f). \tag{2}$$

The broadband L_s for each boat regime was computed by integrating the narrowband pressure spectra for (1) 10–5000 Hz, (2) 89.1–8910 Hz (ADEON band BD), and (3) 8910–22 400 Hz.

To verify our vector sensor calibrations, we compared the measured particle velocity from the sensor with the estimated particle velocity from the sound pressure recorded from the SoundTrap used in this study. In relatively far-field conditions while measuring a single source, the measured particle velocity of the vector sensor should be nearly equal to the estimated values from the hydrophones. We used the plane wave equation to predict the particle motion from the measured sound pressure, as implemented in paPAM version 2.0.11 (Nedelec *et al.*, 2016):

$$v = \frac{p}{\rho c},\tag{3}$$

where v is the particle velocity (m s⁻¹), p is the acoustic pressure (Pa), ρ is the density of the water (1024 kg m⁻³), and is c the sound speed (1480 m s⁻¹). This provides the expected particle velocity measurement assuming an ideal far-field, deep water environment with a plane wave sound field. We present the PSDs that represent the measured particle velocity divided by the estimated particle velocity. These are termed scaled impedance (Ainslie *et al.*, 2024; Oppeneer *et al.*, 2023; Jansen *et al.*, 2019), and in far field conditions, should be close to 0 dB and presented in the supplementary material.

3. Relationship between sound pressure and sound particle motion

To better characterize the acoustic field generated by passing vessels, we examined the relationship between sound pressure and particle velocity. In an ideal plane wave in homogeneous seawater, the ratio |p/v| is constant and equals the characteristic acoustic impedance of the medium, corresponding to $\rho c \approx 1.52 \cdot 10^6 \, Pa \cdot s/m$. Deviations from this reference can reveal departures from ideal plane wave conditions, such as multipath propagation, near-field effects, or complex source–receiver geometries. To estimate the frequency-dependent ratio of sound pressure to particle velocity, a proxy for acoustic impedance magnitude, we calculated the quantity Z(f) as follows:

$$Z(f) = |p(f)/v(f)|, \tag{4}$$

where p(f) and v(f) represent the PSD of sound pressure and tri-axial particle velocity, respectively, in linear units. The PSDs were computed as described above (for frequency band 10–5000 Hz). For each trial, this ratio was computed across all available frequencies. For each speed regime, the distribution of Z(f) was summarized using the 25th, 50th (median), and 75th percentiles across replicate measurements (n=3). These percentiles were calculated at each frequency and plotted as shaded ribbons (interquartile range) with overlaid median lines to illustrate the central tendency and variability of impedance estimates as a function of frequency. To provide a benchmark, a horizontal reference line was added at 1.52 MPa · s/m, corresponding to the characteristic acoustic impedance of seawater.

We also computed root mean square levels in decibels for both components in the 10–5000 Hz band: sound pressure levels ($L_{p,rms}$) were expressed in Pa, and particle velocity levels ($L_{v,rms}$) were expressed in m/s. For each boat pass, the ratio $L_{p,rms}/L_{v,rms}$ was computed, providing

an estimate of how pressure and velocity levels relate on a linear scale.

Finally, to compare measured and theoretical particle motion, we constructed spectrograms from the simultaneously recorded sound pressure and tri-axial accelerometer data from one boat pass (Lili, speed regime 6.5 knots). The measured particle velocity and acceleration spectrograms were generated as described above. Theoretical particle velocity and acceleration were derived from the pressure waveform using a short-time Fourier transform (Hann window, 50% overlap, number of Fourier transform points (NFFT) = 2048). Plane-wave estimates were obtained via the following:

$$v_{pw}(f) = p(f)/\rho c, \tag{5}$$

$$a_{pw}(f) = j2\pi f v_{pw}(f), \tag{6}$$

where $\rho = 1024 \text{ kg m}^{-3}$ and $c = 1500 \text{ m s}^{-1}$. Spherical-wave (monopole) estimates used

$$Z_{sph}(f) = \rho c(1 + j/kr), \tag{7}$$

$$v_{sph}(f) = p(f)/Z_{sph}(f), \tag{8}$$

$$a_{sph}(f) = j2\pi f v_{sph}(f), \tag{9}$$

with $k = 2\pi f/c$ and $r = 20 \,\mathrm{m}$. All velocity levels were expressed in dB re 1 nm s⁻¹ and acceleration levels in dB re 1 $\mu \mathrm{m} \, \mathrm{s}^{-2}$.

III. RESULTS

A total of 155 boat approaches were recorded: 125 recorded by the hydrophone to measure acoustic pressure, and 30 simultaneously recorded with the particle motion sensor. Table I summarizes the recorded boat speed and the approach duration for each boat regime. A total of 56 ambient recordings were taken regularly in between boat approaches: 50 with a hydrophone and six with a particle motion sensor.

Example spectrograms of an ambient recording and a boat approach at each boat regime are shown in Fig. 2. The approach of the boat to the focal recording point is visible in all spectrograms of boat recordings; from a target speed of 6.5 knots (3.33 m/s), boat noise is clearly present from the start of the approach to the end, both in particle acceleration and sound pressure. The signal starts off with frequency and amplitude modulations and becomes more broadband as the source approaches. Peak and trough changes can be observed in the frequency spectrum. These spectrograms illustrate the similarity of boat regimes with each other: while the 3.2 knots (1.67 m/s) spectrogram mostly shows the early appearance of low frequencies (100–1200 Hz), it is hard to distinguish boat regimes from 6.5 to 16.2 knots from each other when the time axes are spread out over the same space, especially on the particle acceleration spectrograms. Inspection of spectrograms from multiple vessel passes (supplementary material) revealed that the prominent hump observed at ~ 1.5 kHz in Fig. 1(b) was not present for all



TABLE I. Mean recorded boat speed, duration, and mean propeller depth for 200 m boat approach at five different boat regimes ± standard error (SE): 3.2 knots (1.67 m/s), 6.5 knots (3.33 m/s), 9.7 knots (5.00 m/s), 13.0 knots (6.67 m/s) and 16.2 knots (8.33 m/s).

Boat speed regime (target speed)	N	Mean recorded speed (± SE) (m/s)	Maximum speed recorded (± SE) (m/s)	Mean recorded approach time (± SE) (s)	Propeller depth (m)
3.2 knots	31	1.7 ± 0.1	2.2 ± 0.1	95.0 ± 0.6	0.61
6.5 knots	31	2.9 ± 0.1	3.7 ± 0.2	54.6 ± 0.5	0.64
9.7 knots	31	4.4 ± 0.1	5.6 ± 0.1	36.1 ± 0.7	0.71
13.0 knots	31	5.6 ± 0.1	7.2 ± 0.1	28.9 ± 0.4	0.74
16.2 knots	31	6.3 ± 0.1	8.5 ± 0.1	25.6 ± 0.3	0.73

vessels. This suggests that the hump is vessel-specific. Such tonal emissions can originate from a variety of mechanical sources, including propeller blade rate harmonics, cavitation, gearbox or engine vibrations, and structural resonances. The presence, frequency, and amplitude of these humps are known to vary depending on vessel type, propulsion system, operational speed, and maintenance condition.

 $L_{p,rms}$, $L_{p,pk}$, L_E , and kurtosis were measured for 122 approaches covering the 5 m to the closest point of approach and 50 ambient recordings, for each boat regime and for two ambient noise durations (0.6 and 3 s), corresponding to the shortest and the longest boat samples, respectively (Table II). Similarly, L_a and $L_{E,a}$ were measured for 31 approaches covering 5 m to the closest point of approach and eight ambient recordings (Table II). While we present these measurements for the frequency band 10–5000 Hz due to hardware limitations of the particle motion sensor, ADEON band BD and the rest of the frequencies are presented in the supplementary material.

For all metrics, boats traveling at 6.5, 9.7, 13.0, and 16.2 knots (3.33, 5.00, 6.67, and 8.33 m/s) have similar values, compared to the 3.2 knots (1.67 m/s) regime which shows higher or lower values, depending on the metric. Kurtosis, which is correlated with a high degree of variation in amplitude in the analyzed sound recording, is much higher (74.23) for 3.2 knots (1.67 m/s) than the rest of the boat regimes, averaging 6.4. This difference is attributed to the domination of ambient noise in the signal (i.e., low signal-to-noise ratio for 3.2 knots), as the ambient noise shows higher kurtosis (between 32 and 300).

The relationships between L_p and L_a for the 10–5000 Hz band and measured boat speed is represented in Fig. 3. Both L_p and L_a increased nonlinearly with mean speed of the boats. These results confirm that, from a certain speed, the sound pressure and particle acceleration levels reach a maximum plateau. Note also the larger imprecision in mean speed at the 16.2 knots (8.33 m/s) regime, probably due to the different load weight in each boat pass (i.e.,

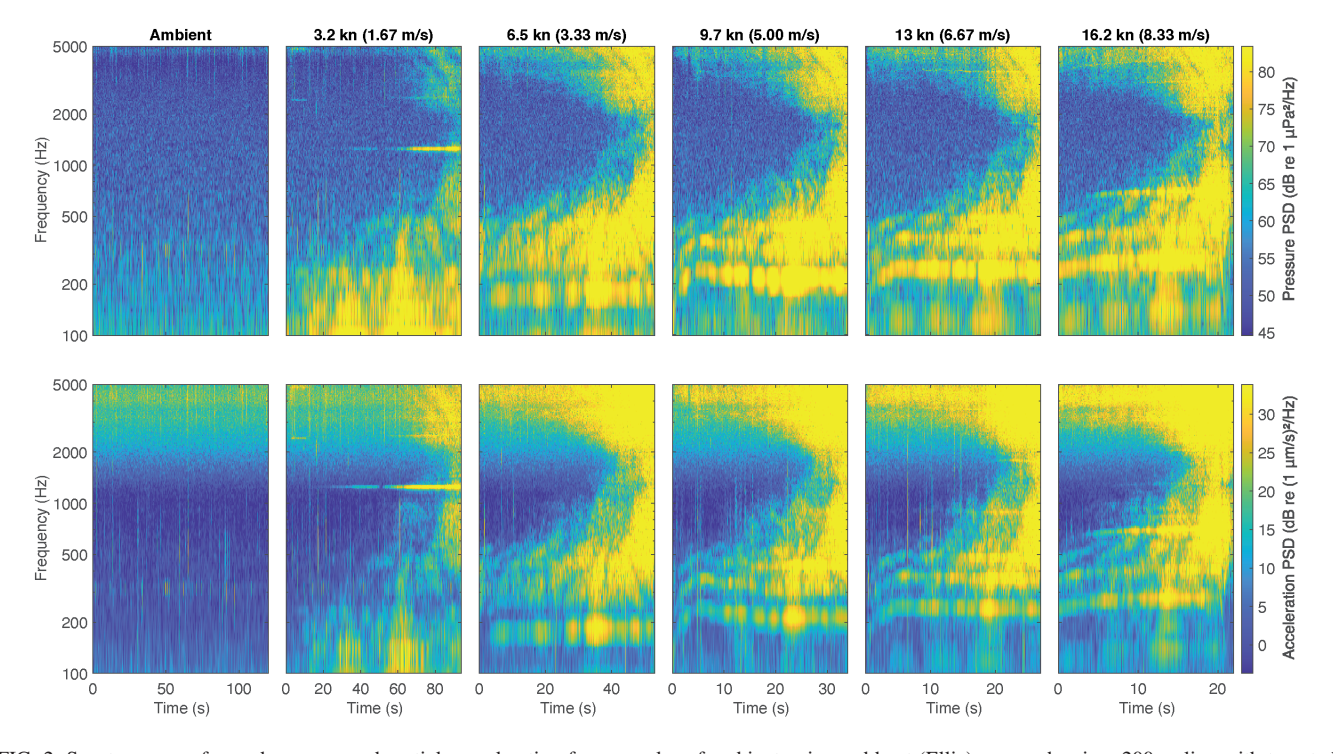


FIG. 2. Spectrograms of sound pressure and particle acceleration for examples of ambient noise and boat (Ellie) approaches in a 200-m line with targeted speed of 3.2 knots (1.67 m/s), 6.5 knots (3.33 m/s), 9.7 knots (5.00 m/s), 13.0 knots (6.67 m/s), and 16.2 knots (8.33 m/s). Both particle acceleration and sound pressure data were bandpass filtered from 10 to 5000 Hz. Spectrograms were built with 42.67 ms Hann windows and 50% overlap.

TABLE II. Mean and standard error for 31 boat approaches and eight ambient recordings of (top) sound pressure level $(L_{p,pms})$, peak sound pressure level $(L_{p,pk})$, sound exposure level (L_{E}) , and sound pressure kurtosis measurements for the recordings of 122 boat approaches at different speed regimes (boat traveling at 3.2, 6.5, 9.7, 13, or 16.2 knots, respectively, 1.67, 3.33, 5.00, 6.67 or 8.33 m/s), recorded 20 m from the source, and 50 ambient noise recordings (recorded for a short duration of 0.6 s or a longer duration of 3 s). Recordings are bandpass filtered from 10 to 5000 Hz. (Bottom) Particle acceleration levels $(L_{a,rms})$ and acceleration exposure level $(L_{E,a})$. All measurements are bandpass filtered from 10 to 5000 Hz. Averaging (for $L_{p,rms}$ and L_a) and integration (for $L_{E,a}$) times correspond to each boat approach duration time (see mean approach time in Table I) \pm standard error.

	Ambient $0.6 \text{ s} \text{ (n} = 25)$	Ambient $3 \text{ s} (n=25)$	3.2 knots (1.67 m/s) (n = 25)	6.5 knots (3.33 m/s) (n = 25)	9.7 knots (5.00 m/s) (n = 25)	13 knots (6.67 m/s) (n = 25)	16.2 knots (8.33 m/s) (n = 25)
$L_{p,rms}$ [dB re 1 μ Pa] $L_{p,pk}$ [dB re 1 μ Pa] L_E [dB re 1 μ Pa ² s] Kurtosis	96.8 ± 1.1 117.3 ± 1.4 95.4 ± 0.7 32.3 ± 9.1	94.9 ± 1.1 122.4 ± 1.6 99.7 ± 0.7 297.0 ± 113.2	112.7 ± 1.1 134.9 ± 1.6 117.5 ± 0.7 74.2 ± 34.8	123.6 ± 0.4 140.8 ± 0.8 125.4 ± 0.4 5.7 ± 0.9	125.0 ± 0.4 140.8 ± 0.8 125.0 ± 0.4 7.5 ± 3.3	125.7 ± 0.9 140.6 ± 0.7 124.5 ± 0.6 4.1 ± 0.3	126.9 ± 0.9 141.4 ± 0.7 124.8 ± 0.7 8.3 ± 4.1
	Ambient 0.6 s $(n=4)$	Ambient 3 s $(n=4)$	3.2 knots (1.67 m/s) $(n = 6)$	6.5 knots (3.33 m/s) $(n = 6)$	9.7 knots $(5.00 \mathrm{m/s})$ $(n=6)$	13 knots (6.67 m/s) $(n = 6)$	16.2 knots (8.33 m/s) $(n = 6)$
$L_{a,rms}$ [dB re 1 μ m s ⁻²] $L_{E,a}$ [dB re 1 μ m ² s ⁻³]	58.4 ± 2.0 54.0 ± 2.0	58.7 ± 2.2 61.4 ± 2.2	69.5 ± 1.3 72.6 ± 1.5	86.6 ± 0.7 86.7 ± 0.7	87.9 ± 0.5 86.2 ± 0.5	89.3 ± 0.8 86.4 ± 0.9	90.7 ± 2.0 86.9 ± 2.0

weight change due to fuel consumption) or the difference in hull cleanliness, having a larger impact at this speed. At this speed range, some of the variability in recorded mean speed could also be attributed to dynamic effects, such as slamming or porpoising motion, which we did not systematically record but may have occurred despite the calm sea state.

The computed PSDs are shown in Fig. 4. They also highlight the similarities between boat speeds 6.5, 9.7, 13, or 16.2 knots (respectively, 3.33, 5.00, 6.67, and 8.33 m/s), whereas 3.2 knots (1.67 m/s) has a distinctive spectrum. All the spectra have peaks/tones between 80 and 600 Hz, which may represent the propeller blade rate and engine firing rate, plus harmonics, as shown in rigid-hulled inflatable boats in Erbe et al. (2016) and other small recreational and fishing boats (Picciulin et al., 2022). Notably, the slowest speed regime studied (3.2 knots) seems to generate the highest spectral density level (> 90 dB) of these low-frequency (<100 Hz) tones, especially visible on the particle acceleration spectrum, whereas

highest spectral density corresponds to high frequencies (>1 kHz) in the fastest regimes.

The estimated source levels for each boat regime for (1) the 10–5000 Hz band, (2) the ADEON band BD (8.91–8910 Hz), and (3) the 8910–22 400 Hz band are shown in Table III. They highlight the similarity between all regimes from and above 9.7 knots.

 L_s are also plotted against the speed of each boat approach (10–5000 Hz, Fig. 5; other frequency bands, supplementary material). There is a nonlinear relationship, with a steep increase in L_s until a speed of about 3 m/s (5.8 knots, 10.8 km/h), then dropping slightly to 5 m/s (9.7 knots, 18 km/h). The relatively large scatter observed in Fig. 5 likely reflects a combination of small environmental variations, slight differences in boat or propeller condition, and the aggregation of frequency-dependent trends across the 10–5000 Hz band. As shown in the supplementary material, variation is relatively small in the 8910–22 400 Hz band

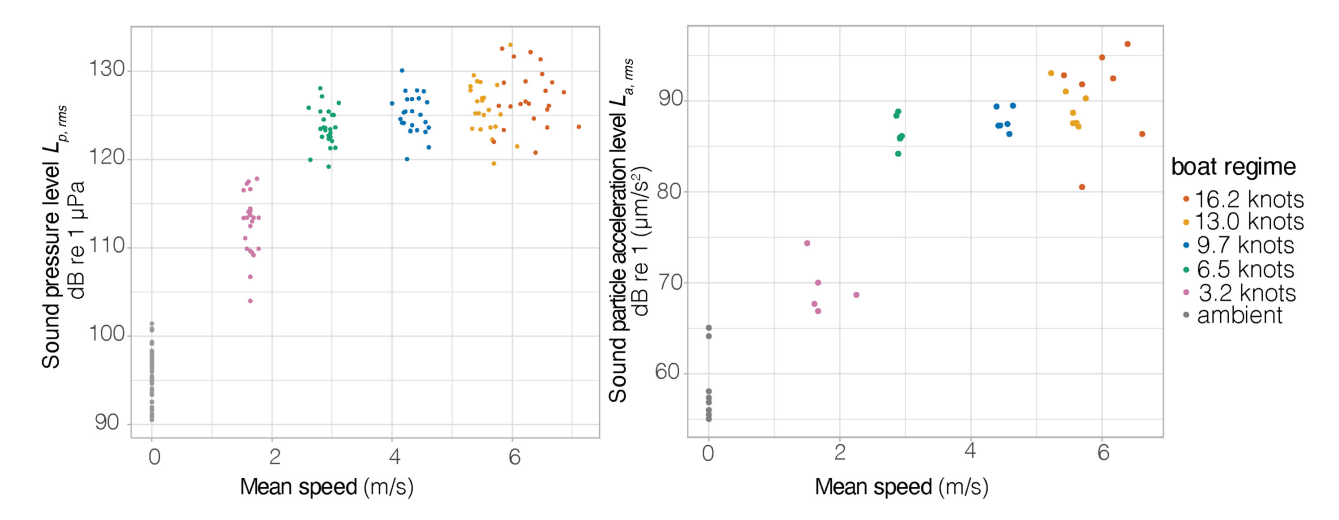


FIG. 3. Sound pressure levels (a: $L_{p,rms}$) and particle acceleration levels (b: $L_{a,rms}$) for bandwidth 10–5000 Hz at recorded mean speeds for each boat regime, recorded as a 5-m approach to the closest point of approach, 20 m away from the source.

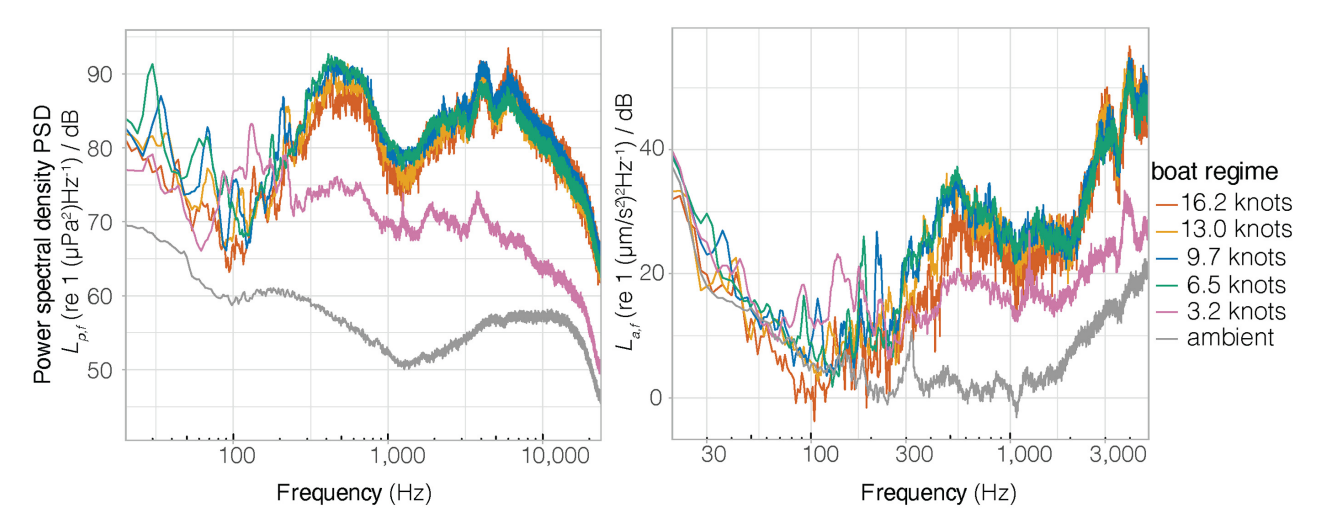


FIG. 4. Power spectral density in sound pressure (left) and particle acceleration (right) for ambient noise and boat approaches with targeted speed of 3.2, 6.5, 9.7, 13, or 16.2 knots, respectively, 1.67, 3.33, 5.00, 6.67, or 8.33 m/s. Fourier transform window duration is 0.5 s, resulting in 2 Hz bands.

but more pronounced in the ADEON band BD (8.91–8910 Hz), suggesting that much of the observed scatter may stem from differences in the lower-frequency components of the signal.

We corrected the PSDs by subtracting the power of ambient noise measured during adjacent time periods under similar environmental conditions. Following this adjustment, source-level PSDs were back-calculated to 1 m by applying cylindrical spreading loss from the measurement distance (20 m). PSDs were computed using a Hann window with a 0.5 s duration and 50% overlap, yielding a 2-Hz resolution. These adjusted spectra are shown in Fig. 6. The highest source spectral density level peak at low frequency (<100 Hz) was 117 dB re 1 μ Pa²m²/Hz in a 2-Hz band (at ~30 Hz, for the 6.5 knots boat speed regime). The 3.2 knots boat regime showed a peak at ~150 Hz (118 dB re 1 μ Pa²m²/Hz), above all the other boat regimes at this frequency.

Across boats and speeds, |p/v| values ranged from 1×10^5 to $1 \times 10^7 \, \mathrm{Pa \cdot s/m}$, generally below the plane wave reference (Fig. 7). Lower speeds tended to yield lower |p/v| values, suggesting weaker correspondence to plane wave behavior under these conditions. Additional analyses of the relationship between particle velocity and acoustic pressure are presented in the supplementary material. Variation between boats was also evident, likely reflecting differences in cleanliness, hull form, and/or propulsion.

To further visualize the relationship between sound pressure and sound particle motion, a scatterplot was

generated where each point represents one boat pass, grouped by vessel ID and plotted against speed regime (Fig. 8). A horizontal dashed line was added at 123.73 dB, corresponding to the expected level difference under free-field plane wave conditions, calculated from the characteristic impedance of seawater ($Z = \rho c = 1.52 \times 10^6 \, \text{Pa} \cdot \text{s/m}$). The measured $L_{p,rms} - L_{v,rms}$ values were consistently below the plane-wave reference, particularly at lower vessel speeds. This suggests that the received field was dominated by near-field or reactive components, where particle velocity is enhanced relative to pressure. As vessel speed increased, the ratio approached the plane-wave value, indicating a larger contribution from the far-field propagating wave.

Finally, new spectrograms were generated to examine the theoretical particle velocity and acceleration derived from the pressure data, with dynamic color limits matched across subplots to facilitate visual comparison. The figure contains six panels: measured velocity, plane wave velocity estimate, spherical-wave velocity estimate, measured acceleration, plane wave acceleration estimate, and spherical-wave acceleration estimate (Fig. 9). The plane- and spherical-wave reconstructions reproduced the timing and dominant spectral bands of the measured particle velocity and acceleration, with close agreement above $\sim\!200\,\mathrm{Hz}$. At lower frequencies, the reconstructions diverged systematically from the measurements, indicating that the simple free-field impedance relations used for the estimates do not fully capture the low-frequency sound field at the site. The

TABLE III. Estimated source level L_s for 10–5000 Hz band, ADEON band BD (8.91–8910 Hz), and 8910–22 400 Hz band, in dB re 1 μ Pa·m for each boat regime.

	Boat regime					
Source level L_s in dB re μ Pa·m	3.2 knots (1.67 m/s)	6.5 knots (3.33 m/s)	9.7 knots (5.00 m/s)	13.0 knots (6.67 m/s)	16.2 knots (8.33 m/s)	
Band 10-5000 Hz	148.1	154.4	151.4	151.6	151.2	
ADEON band BD (8.91–8910 Hz)	148.2	154.6	151.9	152.1	152.1	
Band 8910-22 400 Hz	124.9	136.3	137.8	137.9	140.5	

https://doi.org/10.1121/10.0039578

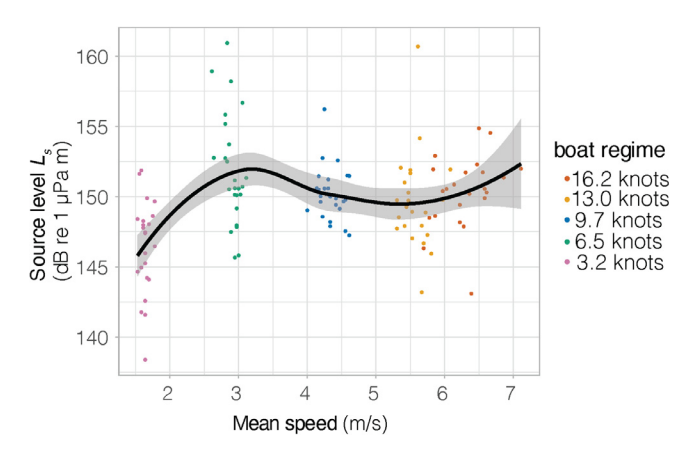


FIG. 5. Source level L_s calculated for the 10–5000 Hz band in relation to the mean speed of each boat pass. A smoothing trend line (black) is fitted with the locally estimated scatterplot smoothing method and formula $y \sim x$. Its gray shadow represents its confidence interval.

low-frequency discrepancies are expected for several reasons. In shallow, bounded coastal waters, the sound field below a few hundred Hertz is strongly influenced by surface—bottom reflections and normal-mode structure, so the local acoustic impedance departs from the free-field values. Second, the vessel is a moving, spatially extended, and directional source (engine/propeller/hull radiation), not a stationary monopole, so the pressure—velocity ratio is source- and geometry-dependent at low frequencies. Third, particle-motion sensors are more susceptible to non-acoustic contamination at low frequency: flow-induced motion around the sensor, mooring/tilt or platform vibrations, and instrument response roll-off can elevate apparent velocity/acceleration PSDs below a few hundred Hertz.

IV. DISCUSSION

We characterized the acoustic footprint of a class of small vessel navigating in shallow coastal waters, at different speeds, in terms of sound pressure and sound particle acceleration. For all metrics calculated ($L_{p,rms}$, $L_{p,pk}$, L_{E} , $L_{a,rms}$, $L_{E,a}$, kurtosis), the lowest speed (3.2 knots or 1.67 m/s) generated a distinct

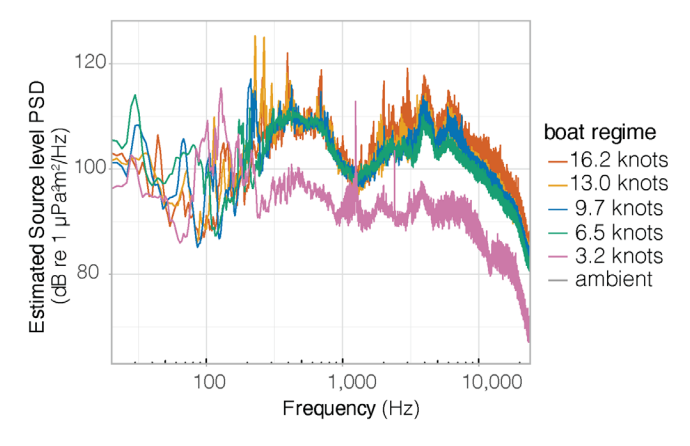


FIG. 6. Estimated source spectral density levels for boat approaches with target speed of 3.2, 6.5, 9.7, 13, or 16.2 knots, respectively, 1.67, 3.33, 5.00, 6.67, or 8.33 m/s. Fourier transform window duration is 0.5 s, resulting in 2 Hz bands.

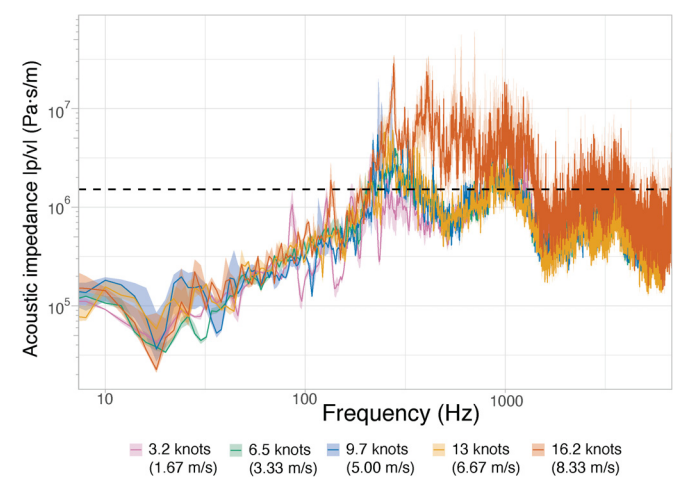


FIG. 7. Frequency-resolved estimate of the acoustic impedance |p/v| in Pa·s/m for each boat speed regime for the spectral band from 10 to 5000 Hz. Lines indicate the median. Shaded bands show the interquartile range (25th–75th percentile) across replicate measurements. This plot provides a comprehensive view of how acoustic impedance varies with both frequency and boat speed. A horizontal dashed line at 1.52 MPa·s/m indicates the expected acoustic impedance of a plane wave in open water, included as a reference for comparison.

signature from all the other speed regimes (6.5, 9.7, 13.0, or 16.2 knots, equivalent to 3.33, 5.00, 6.67 or 8.33 m/s), which showed similar proprieties. We acknowledge that the exclusive focus on the approach phase limits the completeness of our acoustic characterization, particularly considering the sternmounted engine and the potential for horizontal directivity effects during departure. This asymmetry could influence received sound levels in different orientations and should be addressed in future studies designed for full underwater radiated noise assessments (ISO 17208-1:2016, 2016; ISO 17208-3:2023, 2025).

While 16.2 knots (8.33 m/s) was the highest target speed regime considered, $L_{p,rms}$ peaked from 9.7 knots (5.00 m/s)

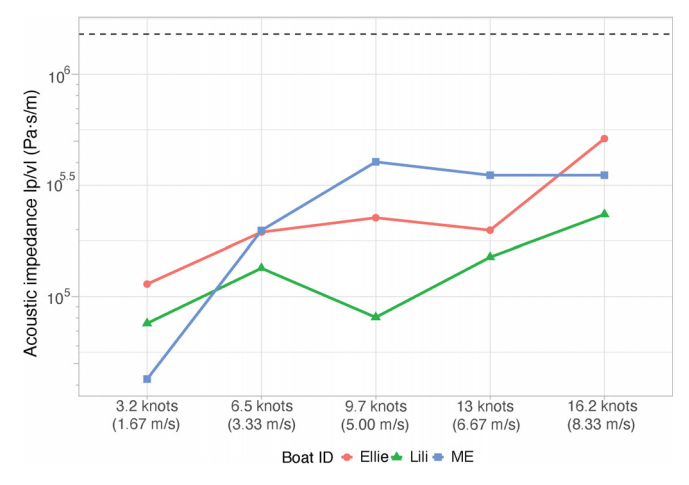


FIG. 8. Acoustic impedance |p/v| across five speed regimes for three boats, band-passed between 10 and 5000 Hz. Each point represents a single boat pass, with shape and color indicating the vessel ID. Lines connect points from the same boat across speed regimes. A dashed horizontal line at $1.51552 \times 10^6 \, \text{Pa} \cdot \text{s/m}$ indicates the theoretical difference expected under ideal free-field plane wave conditions in seawater.

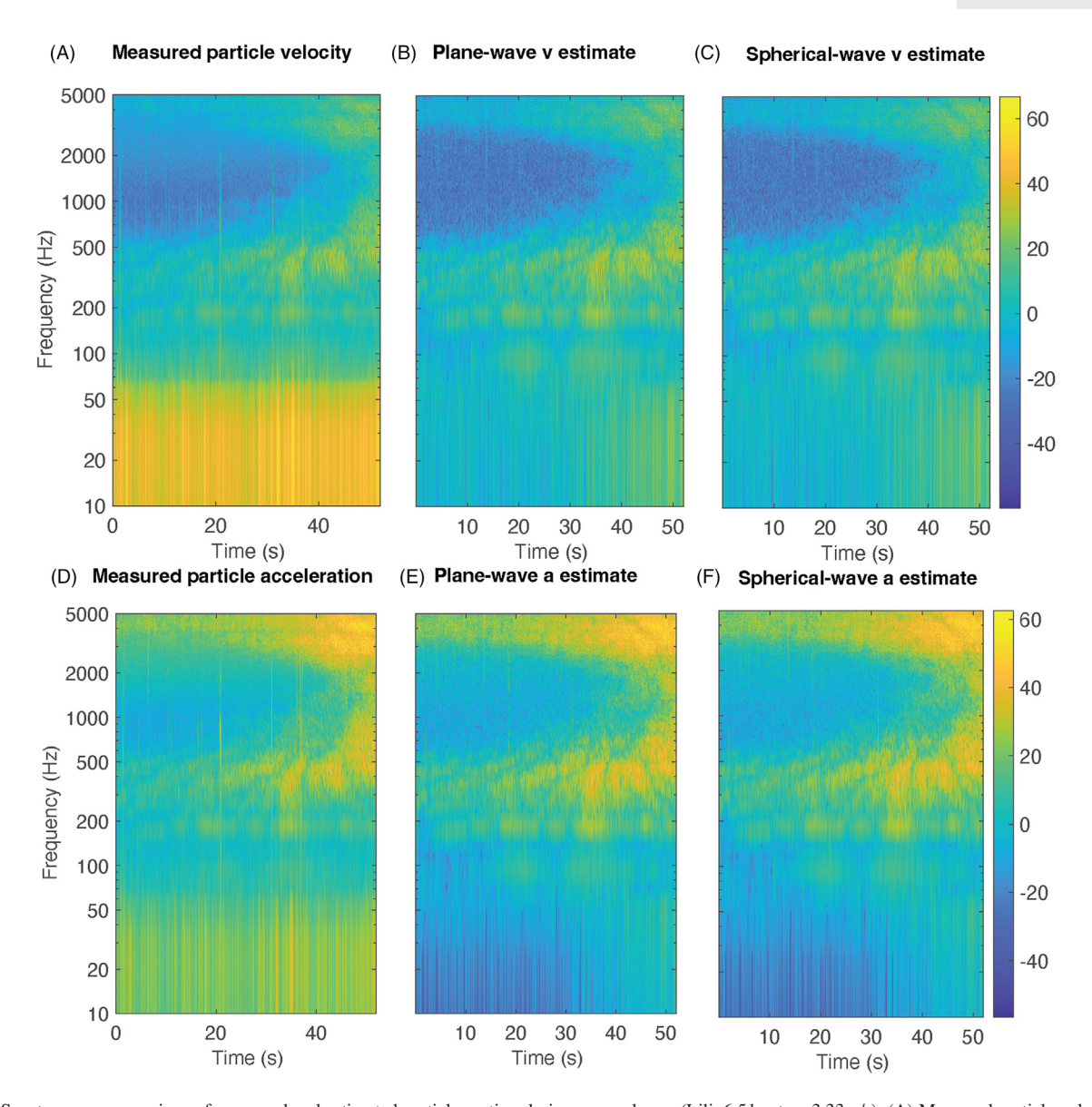


FIG. 9. Spectrogram comparison of measured and estimated particle motion during a vessel pass (Lili, 6.5 knots = 3.33m/s). (A) Measured particle velocity (dB re (1 (nm/s)^2) /Hz) from tri-axial accelerometer data (magnitude xyz). (B) Particle velocity estimated from simultaneous pressure recordings using a plane wave assumption. (C) Particle velocity estimated using a spherical-wave (monopole) model at 20 m range. (D) Measured particle acceleration [dB re $(1 \text{ (}\mu\text{m/s}^2)^2)$ /Hz] from accelerometer data (magnitude xyz). (E) Particle acceleration estimated from pressure under a plane wave assumption. (F) Particle acceleration estimated using a spherical-wave model. All spectrograms use a Hann window (number of Fourier transform points (NFFT) = 2048, 50% overlap) and matched dynamic color limits to enable direct visual comparison between measured and modeled quantities.

and L_a peaked from 13.0 knots (6.67 m/s) (Table II). However, the rise of both $L_{p,rms}$ and $L_{a,rms}$ was not linear (Fig. 3). We show that the acoustic pressure and particle acceleration increase as the boat goes faster but decrease again for still higher speeds. Such stabilizing/decreasing noise levels have also been described for rigid-hulled inflatable boats by Erbe *et al.* (2016). Despite an increase in speed, from 9.7 to 16.2 knots (5 to 8.33 m/s), $L_{p,rms}$ did not increase significantly at these higher speeds. For example, a doubling of the speed from 6.5 to 13 knots (3.33 to 6.67 m/s) corresponds to an increase in only 1.4 dB for the frequency band 10–5000 Hz. By comparison, from ambient levels to 3.2 knots (1.67 m/s), the slowest targeted speed used in this study, $L_{p,rms}$ increased by more than 15 dB (more than

30-fold). The $L_{p,rms}$ and L_a highest levels between 3.2 and 6.5 knots (between 1.67 and 3.33 m/s) may correspond to the point at which the boat's hull encounters the greatest resistance and the propeller experiences its highest loading. Above a certain speed (i.e., 6.5 knots or 3.33 m/s), the boat transitions toward planing, during which the bow lifts out of the water. While this transition does not necessarily imply a drop in hydrodynamic resistance, the rate of increase in resistance typically decreases, and the vessel speed begins to increase more rapidly than the propeller speed, resulting in reduced propeller loading. Other sources of noise, like the vessel slapping on the water from its planing, may be responsible for the small increase observed in $L_{p,rms}$ and $L_{a,rms}$ from 13 to 16.2 knots.

Similarly, the estimated L_s increased steeply from the ambient noise level to 3 m/s ($\sim 5.83 \text{ knots}$), then reaching asymptote for the low-frequency band (10–5000 Hz) (Fig. 3). The correlation between sound levels and boat speed is usually described as positive (Ross, 1976) although the exact relationship is vessel specific (Chion et al., 2019). For this type of small research vessel (5 m length, 2.1 m wide), the L_s seems even to decrease for speeds higher than 6.5 knots (\sim 3.3 m/s). This type of vessel can thus potentially produce more noise at speeds below its optimal cruising speed. In the higher-frequency bands (8910–22400 Hz), the estimated source level increases again for speeds exceeding 6 m/s (11.7 knots) after an equilibrium between 3 and 6 m/s (see supplemental material). This difference highlights the importance of frequency weighting while considering sound exposure levels and the need of weighting functions for different taxa with different hearing sensitivities.

For all speeds, the start of the spectra was characterized by single frequency tones from 80 to 500 Hz (Fig. 4, especially visible for the particle acceleration). These components were particularly noticeable at slow speed (i.e., 3.2 knots), where almost all the energy occurred in the low frequencies, below 200 Hz: although the lowest speed, it shows the highest energy of all boat regimes for frequencies under 200 Hz (Fig. 4). As seen in Picciulin *et al.* (2022), the highest speed may induce highest $L_{p,rms}$ only in a very limited frequency range, depending on the engine type. In small boats, narrowband tones are associated with individual cylinder firings and the overall engine firing rate (Matzner *et al.*, 2010).

As the speed increased, there was a rise of sound level at frequencies 500–10 000 Hz (Fig. 5). This pattern, which is visible both for pressure and particle motion, was previously described by Parsons and Meekan (2020) while testing the noise of vessels of different sizes in a similar environment, and by Smith et al. (2025) for small outboard-powered rigid inflatable boats. The broadband increase could be attributed to the intensity of the cavitation noise, which is related directly to the propeller rotation rate (Ross, 1976), also visible in other studies (Erbe et al., 2016; MacGillivray et al., 2019). As the vessel speed increases, higher-frequency broadband sound may result from a range of hydrodynamic factors, including possible cavitation or turbulence near the propeller. However, for small planing craft, propeller loading typically decreases once the vessel is on plane, and cavitation may not increase with speed in the same manner as in larger displacement vessels (Svedendahl et al., 2021; Smith et al., 2024). These higher frequencies would also propagate better in the shallow environment than the low frequencies (<500 Hz). From a speed of 6.5 knots (3.33 m/s), the characteristics of the boat's regime are all very similar in the frequency domain (Figs. 2-4), and it is hard to distinguish one from the other. This increase was also not strictly linear and was accompanied by considerable variability across passes. This aligns with recent studies that have challenged the assumption of a monotonic relationship between speed and underwater radiated noise in small vessels. For instance,

Svedendahl *et al.* (2021) observed that certain boats emitted higher noise levels at lower speeds due to suboptimal propeller performance and early-onset cavitation, likely because the vessel was not operating at its design cruising speed. Similarly, Smith *et al.* (2024) and Smith *et al.* (2025) demonstrated that propeller fouling and damage can drastically alter cavitation dynamics, producing noise patterns that deviate from expected speed-based scaling. While our study did not include visual assessment of cavitation or propeller condition, the substantial spread in noise levels across boat passes, particularly at fast speeds, suggests that similar mechanisms may be at play. Taken together, these findings emphasize the need to account for vessel-specific characteristics and propeller dynamics when interpreting speed—noise relationships in shallow coastal environments.

Mitigation options for boat noise typically include the slowdown of vessels (Leaper, 2019; MacGillivray et al., 2019; Williams et al., 2019). The drawback of slow vessels is that the overall time of noise exposure is then prolonged. In this study, we included the sound exposure levels to account for the duration of the approach. The exposure levels were the lowest at 3.2 knots (1.67 m/s) and reached their maximum at \sim 6.5 knots (3.33 m/s), for their respective integration time (Table I). Therefore, for these small vessels, slowdowns from high speed to about 6.5 knots (3.33 m/s) could provide a net increase in noise exposure. We also showed that the slow-moving boats produced higher levels of both particle motion and pressure in low frequency tones, which overlap with the sensitivity range of invertebrates and fishes. In this context, driving the boat at planing speed or driving at speeds lower than 6.5 knots (3.33 m/s) may be a better strategy for noise mitigation. In this study, we did not consider the acceleration or deceleration phase of the vessel, although their acoustic dynamics may be important in the context of mitigation. For example, Lagrois et al. (2022) showed that a ferry accelerating or decelerating was one order of magnitude noisier than at operational speed. A vessel's optimal cruising speed, including acceleration and deceleration, should be considered when speed limitations and mitigation measures are considered. Similarly, other parameters than sound level, such as kurtosis, may be important. In this study, kurtosis was significantly higher for the 3.2-knot (1.67 m/s) regime compared to faster speeds, for sound pressure. This suggests that the acoustic signal at low speeds was more impulsive, likely dominated by distinct tonal components, such as engine firing or propeller blade rates. In contrast, higher speeds resulted in lower kurtosis, consistent with broader, more continuous noise profiles dominated by cavitation or turbulence.

We also highlight the importance of considering different frequency bands while calculating sound exposure and estimating source levels. Auditory frequency weighting functions for aquatic organisms can describe the susceptibility to hearing impairments or the relative hearing sensitivity for the studied sound sources within the audible range of each group. Weighting functions have been developed for different groups of marine mammals (Southall *et al.*, 2019)

https://doi.org/10.1121/10.0039578



and of fishes and invertebrates (Lucke *et al.*, 2024). For these taxa in particular, sound particle motion is important to consider and should be measured for more anthropogenic sources.

Our field particle motion measurements diverged from the plane wave predicted values from the SoundTrap, especially for speed higher than 3.2 knots (see the supplementary material): this could be due to the small difference in location between the two sensors (i.e., side by side but separated by \sim 50 cm), the shallow depths, or the reefs present in the area. Across most frequencies, the measured |p/v| ratios ranged from 0.1 to 10 MPa · s/m, with the plane-wave reference (1.52 MPa · s/m) lying near the middle of this range (Fig. 7). Ratios below the reference indicate velocity-rich fields, likely due to near-field or hydrodynamic effects, and were more common at lower frequencies and slower vessel speeds. Ratios close to the reference suggest plane-wavelike behavior, typically observed at mid-frequencies. Ratios above the reference, more common at higher frequencies and faster speeds, indicate pressure dominance, consistent with far-field radiation. These patterns suggest that both frequency and vessel speed influence the balance between pressure and particle velocity in the measured field.

In practice, two important effects cause deviations from the reference value. First, near-field effects, arising within roughly one wavelength of a source, are dominated by reactive energy storage, where particle velocity can be enhanced relative to pressure due to the presence of evanescent and non-propagating components of the sound field. Second, shallow-water propagation constrains acoustic modes between the surface and seabed, altering the local balance of pressure and velocity depending on modal structure, frequency, and measurement geometry. At low frequencies, and especially close to the seabed, particle motion can be amplified relative to pressure due to boundary interactions and mode conversion. Our results show exactly these trends: broadband $L_{p,rms} - L_{v,rms}$ values were consistently below the plane-wave reference (Fig. 8), particularly at lower vessel speeds, indicating stronger relative particle motion. With increasing speed, the difference approached the theoretical plane-wave value, consistent with a shift toward a more farfield-like sound field dominated by propagating modes.

V. CONCLUSION

While we show here that reducing speed does not always reduce the noise exposure, there is early evidence that reducing the speed of this type of motorboat to a very slow speed with no wake can be beneficial to nesting coral reef fish behavior (McCloskey et al., 2020). Thus, reducing motorboat speeds could have a positive impact, if done with thought to the specifics of the vessel. Driving at either very slow (e.g., no wake) or at optimum speed for the hull design (e.g., "on the plane") is also likely to maintain greatest fuel efficiency and comfort for crew, meaning that these factors could aid motorboat drivers making choices about their driving style.

SUPPLEMENTARY MATERIAL

See the supplementary material for further analyses of small vessel noise in shallow waters, including measurements of sound pressure, particle velocity and acceleration across different bandwidths, comparisons of observed and theoretical impedance relationships, and validation of pressure-based estimates of particle motion.

ACKNOWLEDGMENTS

This work was supported by Natural Environment Research Council Research Grant No. NE/P001572/1 to S.D.S. and A.N.R.; Swiss National Science Foundation Early Postdoc Mobility Fellowship P2SKP3-181384 to L.C., and a Royal Society Dorothy Hodgkin Fellowship to S.L.N. We would like to thank the staff at the Lizard Island Research Station for their support to this study, especially co-directors Dr. Anne Hoggett and Dr. Lyle Vail for boat propeller measurements; Bruce Armstrong and Roberto Yubero for generously reviewing the manuscript and providing valuable feedback that significantly improved its clarity and quality.

AUTHOR DECLARATIONS Conflict of Interest

The authors have no conflicts to disclose.

Ethics Approval

Ethical approvals covering the experiments for this project were acquired from Lizard Island Research Station, Great Barrier Reef Marine Park Authority (G39752.1), James Cook University (A2641), and the University of Exeter (eCLESBio000270).

DATA AVAILABILITY

All data and scripts are available upon reasonable request to the authors.

Ainslie, M. A., Andrew, R. K., Howe, B. M., and Mercer, J. A. (2021). "Temperature-driven seasonal and longer term changes in spatially averaged deep ocean ambient sound at frequencies 63–125 Hz," J. Acoust. Soc. Am. 149, 2531–2545.

Ainslie, M. A., Bruiliard, F.-A., de Jong, C. A. F., Diaz, J. A., Folegot, T., Ghasemi, M., Halvorsen, M. B., Slabbekoorn, H., Tougaard, J., and van der Schaar, M. (2024). "SATURN Acoustical Terminology Standard," version 2.0.

Ainslie, M. A., Miksis-Olds, J. L., Martin, B., Heaney, K., de Jong, C. A. F., von Benda-Beckmann, A. M., and Lyons, A. P. (2018). "ADEON Underwater Soundscape and Modeling Metadata Standard," Technical report by JASCO Applied Sciences for ADEON Prime Contract No. M16PC00003.

Blair, H. B., Merchant, N. D., Friedlaender, A. S., Wiley, D. N., and Parks, S. E. (2016). "Evidence for ship noise impacts on humpback whale foraging behaviour," Biol. Lett. 12, 20160005.

Chion, C., Lagrois, D., and Dupras, J. (2019). "A meta-analysis to understand the variability in reported source levels of noise radiated by ships from opportunistic studies," Front. Mar. Sci. 6, 714.

Chou, E., Southall, B. L., Robards, M., and Rosenbaum, H. C. (2021). "International policy, recommendations, actions and mitigation efforts of anthropogenic underwater noise," Ocean Coast Manage. 202, 105427.

- Duarte, C. M., Chapuis, L., Collin, S. P., Costa, D. P., Devassy, R. P., Eguiluz, V. M., Erbe, C., Gordon, T. A. C., Halpern, B. S., Harding, H. R., Havlik, M. N., Meekan, M., Merchant, N. D., Miksis-Olds, J. L., Parsons, M., Predragovic, M., Radford, A. N., Radford, C. A., Simpson, S. D., Slabbekoorn, H., Staaterman, E., Van Opzeeland, I. C., Winderen, J., Zhang, X., and Juanes, F., (2021). "The soundscape of the Anthropocene ocean," Science 371, eaba4658.
- Dunlop, R. A., McCauley, R. D., and Noad, M. J. (2020). "Ships and air guns reduce social interactions in humpback whales at greater ranges than other behavioral impacts," Mar. Pollut. Bull. 154, 111072.
- Dunn, C., Theriault, J., Hickmott, L., and Claridge, D. (2021). "Slower ship speed in the Bahamas due to COVID-19 produces a dramatic reduction in ocean sound levels," Front. Mar. Sci. 8, 673565.
- Dyndo, M., Wiśniewska, D. M., Rojano-Doñate, L., and Madsen, P. T. (2015). "Harbour porpoises react to low levels of high frequency vessel noise," Sci. Rep. 5, 11083.
- Erbe, C., Liong, S., Koessler, M. W., Duncan, A. J., and Gourlay, T. (2016). "Underwater sound of rigid-hulled inflatable boats," J. Acoust. Soc. Am. 139, EL223–EL227.
- Erbe, C., Marley, S. A., Schoeman, R. P., Smith, J. N., Trigg, L. E., and Embling, C. B. (2019). "The effects of ship noise on marine mammals: A review," Front. Mar. Sci. 6, 606.
- European Commission, Marine Strategy Framework Directive (2008). Directive 2008/56/EC of the European Parliament and of the Council of 17 June 2008 establishing a framework for community action in the field of marine environmental policy (Marine Strategy Framework Directive).
- Fakan, E. P., and McCormick, M. I. (2019). "Boat noise affects the early life history of two damselfishes," Mar. Pollut. Bull. 141, 493–500.
- Ferrari, M. C. O., McCormick, M. I., Meekan, M. G., Simpson, S. D., Nedelec, S. L., and Chivers, D. P. (2018). "School is out on noisy reefs: The effect of boat noise on predator learning and survival of juvenile coral reef fishes," Proc. Biol. Sci. 285, 20180033.
- Findlay, C. R., Rojano-Doñate, L., Tougaard, J., Johnson, M. P., and Madsen, P. T. (2023). "Small reductions in cargo vessel speed substantially reduce noise impacts to marine mammals," Sci. Adv. 9, eadf2987.
- Graham, A. L., and Cooke, S. J. (2008). "The effects of noise disturbance from various recreational boating activities common to inland waters on the cardiac physiology of a freshwater fish, the largemouth bass (*Micropterus salmoides*)." Aquat. Conserv. 18, 1315–1324.
- Harding, H., Gordon, T., Hsuan, R., Mackaness, A., Radford, A., and Simpson, S. D. (2018). "Fish in habitats with higher motorboat disturbance show reduced sensitivity to motorboat noise," Biol. Lett. 14, 114.
- Hildebrand, J. A. (2009). "Anthropogenic and natural sources of ambient noise in the ocean," Mar. Ecol. Prog. Ser. 395, 5–20.
- Holt, M. M., Noren, D. P., Dunkin, R. C., and Williams, T. M. (2016). "Comparing the metabolic costs of different sound types in bottlenose dolphins," Proc. Mtgs. Acoust. 27, 010019.
- International Maritime Organization (2014). "Guidelines for the Reduction of Underwater Noise from Commercial Shipping to Address Adverse Impacts on Marine Life" (International Maritime Organization, London, UK).
- ISO 1683:2015 (**2015**). "Acoustics: Preferred reference values for acoustical and vibratory levels" (International Organization for Standardization. Geneva, Switzerland).
- ISO 17208-1:2016 (2016). "Acoustics: Quantities and procedures for description and measurement of underwater sound from ships: 1. General requirements for measurements in deep water" (International Organization for Standardization. Geneva, Switzerland).
- ISO 18405:2017 (2017). "Underwater acoustics: Terminology" (International Organization for Standardization. Geneva, Switzerland).
- ISO 7605:2025 (2025). "Underwater acoustics: Measurement of underwater ambient sound" (International Organization for Standardization. Geneva, Switzerland).
- ISO 17208-3:2023 (2025). "Acoustics: Quantities and procedures for description and measurement of underwater sound from ships: 3. Requirements for measurements in shallow water" (International Organization for Standardization. Geneva, Switzerland).
- Ivanova, S. V., Kessel, S. T., Espinoza, M., McLean, M. F., O'Neill, C., Landry, J., Hussey, N. E., Williams, R., Vagle, S., and Fisk, A. T. (2020). "Shipping alters the movement and behavior of Arctic cod (*Boreogadus saida*), a keystone fish in Arctic marine ecosystems," Ecol. Appl. 30, e02050.

- Jain-Schlaepfer, S., Fakan, E., Rummer, J. L., Simpson, S. D., and McCormick, M. I. (2018). "Impact of motorboats on fish embryos depends on engine type," Conserv. Physiol. 6, coy014.
- Jansen, E., Prior, M., and Brouns, E. (2019). "On the conversion between sound pressure and particle motion," Proc. Mtgs. Acoust. 37, 070012.
- Jensen, F. B., Kuperman, W. A., Porter, M. B., and Schmidt, H. (2011). Computational Ocean Acoustics, 2nd ed. (Springer, New York).
- Joy, R., Tollit, D., Wood, J., MacGillivray, A., Li, Z., Trounce, K., and Robinson, O. (2019). "Potential benefits of vessel slowdowns on endangered southern resident killer whales," Front. Mar. Sci. 6, 344.
- Lagrois, D., Chion, C., Sénécal, J.-F., Kowalski, C., Michaud, R., and Vergara, V. (2022). "Avoiding sharp accelerations can mitigate the impacts of a Ferry's radiated noise on the St. Lawrence whales," Sci. Rep. 12, 12111.
- Lagrois, D., Kowalski, C., Sénécal, J.-F., Martins, C. C. A., and Chion, C. (2023). "Low-to-mid-frequency monopole source levels of underwater noise from small recreational vessels in the St. Lawrence Estuary beluga critical habitat," Sensors 23, 1674.
- Leaper, R. (2019). "The role of slower vessel speeds in reducing greenhouse gas emissions, underwater noise and collision risk to whales," Front. Mar. Sci. 6, 505.
- Lecchini, D., Bertucci, F., Gache, C., Khalife, A., Besson, M., Roux, N., Berthe, C., Singh, S., Parmentier, E., Nugues, M. N., Brooker, R. M., Dixson, D. L., and Hédouin, L. (2018). "Boat noise prevents soundscapebased habitat selection by coral planulae," Sci. Rep. 8, 9283.
- Lemos, L. S., Haxel, J. H., Olsen, A., Burnett, J. D., Smith, A., Chandler, T. E., Nieukirk, S. L., Larson, S. E., Hunt, K. E., and Torres, L. G. (2022). "Effects of vessel traffic and ocean noise on gray whale stress hormones," Sci. Rep. 12, 18580.
- Lucke, K., MacGillivray, A. O., Halvorsen, M. B., Ainslie, M. A., Zeddies, D. G., and Sisneros, J. A. (2024). "Recommendations on bioacoustical metrics relevant for regulating exposure to anthropogenic underwater sound," J. Acoust. Soc. Am. 156(4), 2508–2526.
- MacGillivray, A. O., Li, Z., Hannay, D. E., Trounce, K. B., and Robinson, O. M. (2019). "Slowing deep-sea commercial vessels reduces underwater radiated noise," J. Acoust. Soc. Am. 146, 340–351.
- MacGillivray, A. O., Martin, S. B., Ainslie, M. A., Dolman, J. N., Li, Z., and Warner, G. A. (2023). "Measuring vessel underwater radiated noise in shallow water," J. Acoust. Soc. Am. 153, 1506–1524.
- Matzner, S., Maxwell, A., Myers, J., Caviggia, K., Elster, J., Foley, M., Jones, M., Ogdenz, G., Sorensenz, E., Zurkz, L., Tagestady, J., Stephan, A., Petersony, M., and Bradley, D. (2010). "Small vessel contribution to underwater noise," in *Oceans 2010 MTS IEEE*, Seattle, WA.
- McCloskey, K. P., Chapman, K. E., Chapuis, L., McCormick, M. I., Radford, A. N., and Simpson, S. D. (2020). "Assessing and mitigating impacts of motorboat noise on nesting damselfish," Environ. Pollut. 266, 115376.
- McWhinnie, L., Smallshaw, L., Serra-Sogas, N., O'Hara, P. D., and Canessa, R. (2017). "The grand challenges in researching marine noise pollution from vessels: A horizon scan for 2017," Front. Mar. Sci. 4, 31.
- Mikkelsen, L., Johnson, M., Wisniewska, D. M., Neer, A., van, Siebert, U., Madsen, P. T., and Teilmann, J. (2019). "Long-term sound and movement recording tags to study natural behavior and reaction to ship noise of seals," Ecol. Evol. 9, 2588–2601.
- Mills, S. C., Beldade, R., Henry, L., Laverty, D., Nedelec, S. L., Simpson, S. D., and Radford, A. N. (2020). "Hormonal and behavioural effects of motorboat noise on wild coral reef fish," Environ. Pollut. 262, 114250.
- Müller, R. A. J., Benda-Beckmann, A. M., von, Halvorsen, M. B., and Ainslie, M. A. (2020). "Application of kurtosis to underwater sound," J. Acoust. Soc. Am. 148, 780–792.
- Nedelec, S., Ainslie, M. A., Andersson, M. H., Cheong, S. H., Halvorsen, M. B., Linné, M., Martin, B., Nöjd, A., Robinson, S. P., Simpson, S. D., Wang, L., and Ward, J. (2021). Best Practice Guide for Underwater Particle Motion Measurement for Biological Applications (University of Exeter for the IOGP Marine Sound and Life Joint Industry Programme, Exeter, UK).
- Nedelec, S. L., Campbell, J., Radford, A. N., Simpson, S. D., and Merchant, N. D. (2016). "Particle motion: The missing link in underwater acoustic ecology," Methods Ecol. Evol. 7, 836–842.
- Nedelec, S. L., Mills, S. C., Radford, A. N., Beldade, R., Simpson, S. D., Nedelec, B., and Cote, I. M. (2017a). "Motorboat noise disrupts cooperative interspecific interactions," Sci. Rep. 7, 6987.

https://doi.org/10.1121/10.0039578



- Nedelec, S. L., Radford, A. N., Pearl, L., Nedelec, B., McCormick, M. I., Meekan, M. G., and Simpson, S. D. (2017b). "Motorboat noise impacts parental behaviour and offspring survival in a reef fish," Proc. Biol. Sci. **284** 20170143
- Oppeneer, V. O., de Jong, C. A. F., Binnerts, B., Wood, M. A., and Ainslie, M. A. (2023). "Modelling sound particle motion in shallow water," J. Acoust. Soc. Am. 154, 4004–4015.
- Parsons, M., and Meekan, M. (2020). "Acoustic characteristics of small research vessels," J. Mar. Sci. Eng. 8, 970.
- Picciulin, M., Armelloni, E., Falkner, R., Rako-Gospić, N., Radulović, M., Pleslić, G., Muslim, S., Mihanović, H., and Gaggero, T. (2022). "Characterization of the underwater noise produced by recreational and small fishing boats (<14m) in the shallow-water of the Cres-Lošinj Natura 2000 SCI," Mar. Pollut. Bull. 183, 114050.
- Popper, A. N., and Hawkins, A. D. (2018). "The importance of particle motion to fishes and invertebrates," J. Acoust. Soc. Am. 143, 470–488.
- Popper, A. N., Hawkins, A. D., and Thomsen, F. (2020). "Taking the animals' perspective regarding anthropogenic underwater sound," Trends Ecol Evol. 35, 787-794.
- Putland, R. L., Merchant, N. D., Farcas, A., and Radford, C. A. (2018). "Vessel noise cuts down communication space for vocalizing fish and marine mammals," Global Change Biol. 24, 1708–1721.
- R Core Team. (2019). R: A Language and Environment for Statistical Computing (R Foundation for Statistical Computing, Vienna, Austria).
- Robinson, S., Harris, P., Cheong, S.-H., Wang, L., Livina, V., Haralabus, G., Zampolli, M., and Nielsen, P. (2023). "Impact of the COVID-19 pandemic on levels of deep-ocean acoustic noise." Sci. Rep. 13, 4631.
- Rolland, R. M., Parks, S. E., Hunt, K. E., Castellote, M., Corkeron, P. J., Nowacek, D. P., Wasser, S. K., and Kraus, S. D. (2012). "Evidence that ship noise increases stress in right whales," Proc. Biol. Sci. 279, 2363-2368.
- Ross, D. (1976). Mechanics of Underwater Noise (Peninsula Publishing, Los Altos, CA).
- Shipton, M., Obradović, J., Ferreira, F., Mišković, N., Bulat, T., Cukrov, N., and Diamant, R. (2025). "A database of underwater radiated noise from small vessels in the coastal area," Sci. Data 12(1), 289.
- Simpson, S. D., Radford, A. N., Nedelec, S. L., Ferrari, M. C. O., Chivers, D. P., McCormick, M. I., and Meekan, M. G. (2016). "Anthropogenic noise increases fish mortality by predation," Nat. Commun. 7, 10544.
- Slabbekoorn, H., Bouton, N., van Opzeeland, I., Coers, A., ten Cate, C., and Popper, A. N. (2010). "A noisy spring: The impact of globally rising underwater sound levels on fish," Trends Ecol. Evol. 25, 419–427.
- Smith, T. A., Rosa, A. G. L., Piggott, G., Gaivota, J. A. N., and McMorran, S. S. (2025). "Propeller cavitation on small craft: Underwater noise measurements and visualisation from full-scale trials," Ocean Eng. 317, 120024.
- Smith, T. A., Rosa, A. G. L., and Wood, B. (2024). "Underwater radiated noise from small craft in shallow water: Effects of speed and running attitude," Ocean Eng. 306, 118040.

- Solé, M., Kaifu, K., Mooney, T. A., Nedelec, S. L., Olivier, F., Radford, A. N., Vazzana, M., Wale, M. A., Semmens, J. M., Simpson, S. D., Buscaino, G., Hawkins, A., Aguilar de Soto, N., Akamatsu, T., Chauvaud, L., Day, R. D., Fitzgibbon, Q., McCauley, R. D., and André, M. (2023). "Marine invertebrates and noise," Front. Mar. Sci. 10, 1129057.
- Southall, B. L., Finneran, J. J., Reichmuth, C., Nachtigall, P. E., Ketten, D. R., Bowles, A. E., Ellison, W. T., Nowacek, D. P., and Tyack, P. L. (2019). "Marine mammal noise exposure criteria: Updated scientific recommendations for residual hearing effects," Aquat. Mamm. 45, 125-232.
- Southall, B. L., Nowacek, D. P., Bowles, A. E., Senigaglia, V., Bejder, L., and Tyack, P. L. (2021). "Marine mammal noise exposure criteria: Assessing the severity of marine mammal behavioral responses to human noise," Aquat. Mamm. 47, 421-464.
- Stanley, J. A., Parijs, S. M. V., and Hatch, L. T. (2017). "Underwater sound from vessel traffic reduces the effective communication range in Atlantic cod and haddock," Sci. Rep. 7, 14633.
- Svedendahl, M., Lalander, E., Sigray, P., Östberg, M., and Andersson, M. (2021). "Underwater acoustic signatures from recreational boats: Field measurement and guideline", FOI report FOI-R-5115-SE, Stockholm,
- Vabø, R., Olsen, K., and Huse, I. (2002). "The effect of vessel avoidance of wintering Norwegian spring spawning herring," Fish. Res. 58, 59–77.
- Wale, M. A., Simpson, S. D., and Radford, A. N. (2013). "Noise negatively affects foraging and antipredator behaviour in shore crabs," Anim. Behav. **86**, 111–118.
- Wenz, G. M. (1962). "Acoustic ambient noise in the ocean: Spectra and sources," J. Acoust. Soc. Am. 34, 1936–1956.
- Whitfield, A. K., and Becker, A. (2014). "Impacts of recreational motorboats on fishes: A review," Mar. Pollut. Bull. 83, 24-31.
- Wickham, H. (2016). ggplot2: Elegant Graphics for Data Analysis (Springer-Verlag, New York).
- Williams, R., Veirs, S., Veirs, V., Ashe, E., and Mastick, N. (2019). "Approaches to reduce noise from ships operating in important killer whale habitats," Mar. Pollut. Bull. 139, 459-469.
- Wilson, L., Pine, M. K., and Radford, C. A. (2022). "Small recreational boats: A ubiquitous source of sound pollution in shallow coastal habitats," Mar. Pollut. Bull. 174, 113295.
- Wisniewska, D. M., Johnson, M., Teilmann, J., Siebert, U., Galatius, A., Dietz, R., and Madsen, P. T. (2018). "High rates of vessel noise disrupt foraging in wild harbour porpoises (Phocoena phocoena)." Proc. Biol. Sci. 285, 20172314.
- Wysocki, L. E., Dittami, J. P., and Ladich, F. (2006). "Ship noise and cortisol secretion in European freshwater fishes," Biol. Conserv. 128, 501–508.
- Yubero, R., de Jong, C. A. F., Ainslie, M. A., MacGillivray, A. O., and Wang, L. (2025). "Measuring vessel source level in shallow water using the smoothed semi-coherent image method," J. Acoust. Soc. Am. 157, 1938-1954.